


Growth modes of quasicrystals involving intermediate phases and a multistep behavior studied by phase field crystal model

Zhencheng Jiang ¹, Silong Quan,^{1,2} Ning Xu,³ Linghui He,^{1,4} and Yong Ni^{1,4,*}

¹CAS Key Laboratory of Mechanical Behavior and Design of Materials, Department of Modern Mechanics, University of Science and Technology of China, Hefei 230026, People's Republic of China

²School of Mechanical and Electronic Engineering, East China University of Technology, Nanchang 330013, People's Republic of China

³Hefei National Laboratory for Physical Sciences at the Microscale, CAS Key Laboratory of Microscale Magnetic Resonance, and Department of Physics, University of Science and Technology of China, Hefei 230026, People's Republic of China

⁴CAS Center for Excellence in Complex System Mechanics



(Received 14 October 2019; accepted 4 February 2020; published 26 February 2020)

Understanding the microscopic kinetics of quasicrystal formation via nucleation and growth is crucial. Here, we report unusual pathways to nucleation and growth of dodecagonal quasicrystals via a phase field crystal model incorporating a two-length-scale potential. Under certain thermodynamic parameters, both quasicrystal growths via heterogeneous and homogeneous nucleation may be associated with a multistep behavior and the transient appearance of triangular and intermediate phases, different from classical nucleation pathways. The metastable intermediate phase spontaneously occurs to bridge the triangular phase and quasicrystal nuclei of different orientations to reduce the total free energy of the system. Decomposition of an undercooled fluid phase into quasicrystal phase shows a multistep pathway wherein the triangular phase and the intermediate phase may occur faster than the quasicrystal phase, when the growth rate of one length-scale ordering is significantly different from the other and the subsequent competing and coupling of both length scales are involved. The calculated structure factor, radial distribution function, and the aperiodic tiling structure of the intermediate phase explain why it appears during the quasicrystal formation.

DOI: [10.1103/PhysRevMaterials.4.023403](https://doi.org/10.1103/PhysRevMaterials.4.023403)

I. INTRODUCTION

Quasicrystal (QC) as a structure with quasi-periodic long-range order and no translational order, has attracted substantial interest in materials science and condensed matter physics since its first discovery [1,2]. To this date, thousands of QCs with five-, eight-, ten-, 12-, 18-fold rotational symmetries have been reported, mostly in metallic alloys [3] and recently in soft matter systems [4–10]. The conditions for the formation of stable QCs have been revealed from specific factors of different physical natures to common principles in different QCs [3,11]. The geometric feature of QCs is usually described by the abstract tiling rules, such as Penrose tiling and random tiling model [12]. The stability of QCs is attributed to be a low free energy state by a compromise between configuration entropy and interaction energy between particles with specific pair potential, wherein competing and nonlinear interactions of at least two length scales are crucial [13–20].

Besides the efforts to investigate the existence and stabilities of QCs geometrically and thermodynamically, it has become attractive to investigate possible practical growth mechanisms that can contribute to a structure with long-range aperiodicity and how structural phase transitions proceed from and to the quasicrystalline state (see Refs. [11,21] and references therein). In comparison with the growth of periodic ordering by repeating a regular unit cell, QCs due to their

structural aperiodicity exhibit more complex growth behavior. In general, two categories for QCs' growth rules have been proposed: energy-driven defect-free structure models [22] and entropy-driven random tiling models [23]. By using phase field simulations, the pathways of defect-free QC growth and random tiling-like QC growth have been discovered [24]. In particular, molecular dynamics (MD) simulations demonstrate that icosahedral clusters form in the liquid first and then are incorporated into the growth front of dodecagonal QC nuclei to contribute to the growth of QCs [25], which indicates a two-step growth mode. Archer *et al.* demonstrated that a transient small scale crystal structure emerged during a deep quench of the initially unstable uniform liquid into a QC by performing dynamical density functional simulations in two dimensions [26,27]. Interestingly, Mikhael *et al.* [28,29] discovered an $(3^2 \cdot 4^2)$ Archimedean-like tiling structure with aperiodicity in one direction as an intermediate state between a decagonal QC and a triangular crystal by studying the phase behavior of a colloidal monolayer interacting with tunable optical quasicrystalline substrate. A similar Archimedean tiling cluster has also been reported as a bridge “wetting layer” during the transition from the dodecagonal QC phase to cubic phase in binary nanoparticles superlattices system [6]. All of these findings indicate that growth of QCs may occur in a multistep manner via some intermediate or metastable states. In fact, similar multistage mechanisms have been widely reported in various nucleating systems [30–32], including, but not limited to decomposition in alloys [33–39], crystallization [40–44], and structural transformation in colloidal crystals

*Corresponding author: yni@ustc.edu.cn

[45], wherein appearance and subsequent transformation of intermediate states before reaching a thermodynamically stable phase is universal.

Recently molecular dynamics simulation has been applied to explore the growth processes of two-dimensional (2D) quasicrystals, limited by time and space scales [16,18,19,25,46]. The so-called phase-field crystal (PFC) modeling shows the advantage of modeling microstructure evolution with atomic resolution and diffusive time scales [47,48]. This model is similar to the atomic density function theory proposed by Jin and Khachatryan [49]. Originally the free energy expression of the phenomenological PFC model is based on an expansion of the Swift-Hohenberg free energy [50,51], but later it was proved that it can be derived from density functional theory (DFT) [52,53]. After constructing the phenomenological free energy function for crystalline states with multiple competing length scales, the developed so-called multimode PFC model is capable of formation of more complex ordered structures [54–56], nucleation dynamics [32,42,43,54] and structural phase transformations [55,56], although some modifications [57–60] are made to more accurately describe the defects' behavior, which is, nevertheless, only suitable to the system containing single kind of symmetry lattice by far. In particular, 2D or three-dimensional (3D) quasicrystalline structures can be recovered when a potential with two competing length scales is incorporated in the framework of PFC or DFT [17,24,26,61,62].

Here, given the lack of understanding the multistep metastable growth mechanism of QCs, we employ a PFC model with a two-length-scale potential [24] to comprehensively investigate the growth behavior of QCs involving intermediate phase and multistep behavior, wherein we do not specify any quasicrystal materials. By studying different cases of heterogeneous nucleation followed by growth and growth dynamics in a decomposition of the undercooled liquid into a QC phase, we discover a multistep transition behavior via two metastable solid states, i.e., triangular (Tri) structure and intermediate (Int) structure (the term ‘‘Int’’ refers to the specific phase we found in the text). Especially, analyses of the static structure factor and the radial distribution function indicate that the Int phase serves as a structurally compromised metastable state between the Tri and QC phases and is revealed to possess a 2D structure with aperiodicity in one direction, which is inherent in the two-length-scale model. The correlation and competition between two length scale orderings play an essential role in this multistep phenomenon. Moreover, the PFC model of diffusive time scale enables us to study the complex kinetics and morphology of QCs, such as the movement of defects and growth rate of nuclei.

This article is organized as follows: In Sec. II, the employed two-mode PFC model that incorporates a two-length-scale potential is introduced. The derivation of its dispersion relation based on linear stability analysis is given. Section III presents a modified phase diagram containing liquid, Tri, Int, and QC phases with respect to two parameters, and determines the parameter values for the formation of stable QCs. Different nucleation and growth modes of QCs from an undercooled liquid are simulated. Furthermore, the static structure factor, radial distribution function and the aperiodic tiling structure of the Int phase are analyzed to

elucidate the QC growth mode involving a multistep behavior and an Int phase. Finally, conclusions are marked in Sec. IV.

II. THEORY AND METHOD

A. Two-mode PFC model

The PFC model introduced here is based on a dimensionless free energy functional containing two length scales [24],

$$F[\psi(\vec{r})] = \int d\vec{r} \left\{ \frac{1}{2} \psi(\vec{r}) \left[-\varepsilon + \prod_{m=1}^2 ((k_m^2 + \nabla^2)^2 + b_m) \right] \psi(\vec{r}) + \frac{1}{4} \psi(\vec{r})^4 \right\}, \quad (1)$$

which is generalized from the two-mode form proposed before [14,54], wherein $\psi(\vec{r}, t)$ is a field variable related to atomic density and ε can be interpreted as the mean-field temperature [48]. By changing the two inherent length scales characterized by two wave numbers k_1, k_2 , phases of different symmetries can be controlled. The parameter b_m controls the relative magnitude of different modes. A conserved dynamic equation on diffusive time scales governs the evolution of $\psi(\vec{r}, t)$,

$$\frac{\partial \psi}{\partial t} = \Gamma \nabla^2 \frac{\delta F}{\delta \psi} + \eta, \quad (2)$$

where Γ is the mobility parameter and η is the Gaussian random noise mimicking thermal fluctuation.

Here, to model QCs, two incommensurate length scales are required and the ratio of k_1 and k_2 should be a special value. If we set $k_1 = 2\pi/a$ and $k_2 = 4\pi \cos(\pi/12)/a$, where a is a characteristic length scale, this leads to a stable QC with 12-fold symmetry [14,24], which is a so-called dodecagonal QC. Besides the temperature term ε , another intrinsic term to determine the phase behavior of this model is the mean density $\bar{\psi}$, which is conserved under the dynamical process described by Eq. (2). By numerically solving Eq. (2), the growth behavior of the QCs can be captured through tracking the atomic density field $\psi(\vec{r}, t)$. As for the numerical calculations, a semi-implicit spectral method [63] is used to solve the dynamic equation Eq. (2). All simulations in this paper are conducted with periodic boundary conditions, where the grid space is $\Delta x = a/3\pi$ and dimensionless time step is $\Delta t = 0.1$. Without specific notation, the simulations are conducted in the domain of $1024\Delta x \times 1024\Delta x$. We have tried different sizes of the simulation box (from 512^2 to 2048^2) and found the multistep growth phenomena in all of them, so we believe that the artificial size effect due to periodic boundary conditions can be neglected in the size range we selected. All the density field values of the simulated results are scaled from 0 for the minimum to 1 for the maximum.

B. Linear stability analysis

Before exploring the growth behavior of the QCs during the nucleation process using the PFC simulation, we employ a linear stability analysis of Eq. (2) to study the growth rate of nucleation during the earliest stage of a uniform liquid state [26,49,64]. We firstly assume that the atomic density field ψ has a uniform profile plus an additional small-amplitude

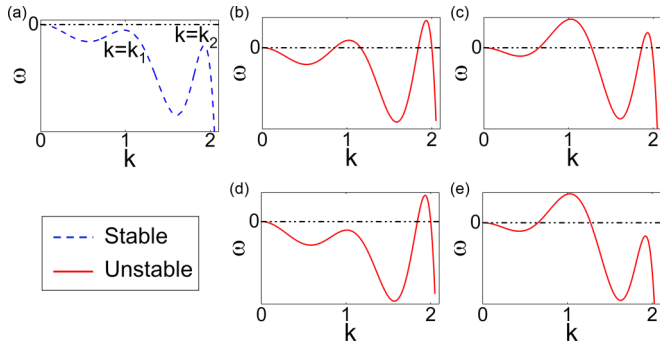


FIG. 1. Dispersion relation of stable (a) and unstable (b)–(e) cases. (a) $\omega(k_1) < 0$, $\omega(k_2) < 0$; (b) $\omega(k_2) > \omega(k_1) > 0$; (c) $\omega(k_1) > \omega(k_2) > 0$; (d) $\omega(k_1) < 0 < \omega(k_2)$; (e) $\omega(k_2) < 0 < \omega(k_1)$.

harmonic perturbation with wave number \vec{k} and angular frequency ω :

$$\psi = \bar{\psi} + \delta\psi = \bar{\psi} + \xi e^{i\vec{k}\cdot\vec{x}} e^{\omega t}, \quad (3)$$

where the amplitude of the perturbation $\xi e^{\omega t}$ is assumed to be an exponential form with $|\xi| \ll 1$. Substituting this expression into the functional derivative of the two-mode free energy (1), we have

$$\frac{\delta F(\psi)}{\delta \psi} = \Lambda \bar{\psi} + \bar{\psi}^3 + (\Lambda + 3\bar{\psi}^2)\delta\psi + O(\delta\psi^2), \quad (4)$$

where $\Lambda = -\varepsilon + \prod_{m=1}^2 [(k_m^2 - k^2)^2 + b_m]$. Then by inserting expression (4) into Eq. (2) and linearizing, the following dispersion relation can be obtained:

$$\omega(k) = -k^2(\Lambda + 3\bar{\psi}^2). \quad (5)$$

The uniform liquid state is linearly stable when $\omega(k) < 0$, while linearly unstable when $\omega(k) > 0$, which means that any small-amplitude perturbation of the wave vector amplifies over time and changes the initial density field configuration, and finally triggers the nucleation and growth behavior. As described by Eq. (5), there are two local maxima, $\omega(k_1)$ and $\omega(k_2)$, in the limit of $k > 0$, corresponding to the fastest growth rate of the perturbation with its characteristic wave numbers k_1, k_2 (see Fig. 1).

Consider the case $(b_1, b_2) = (0, 0)$, by solving the equation $\omega(k) = 0$ of expression (5), we have the relation $-\varepsilon + 3\bar{\psi}^2 = 0$, which defines the linear instability threshold where these two local maxima of $\omega(k)$ both equal zero. Based on this threshold, we find values of the two peaks exhibit $\omega(k_2) < \omega(k_1) < 0$ with lower ε [Fig. 1(a)], while $\omega(k_2) > \omega(k_1) > 0$ on the other side [Fig. 1(b)]. If we choose an appropriate value of ε above the instability threshold, the structure ordering with the period k_2 are expected to appear first. Moreover, we note that the parameters b_1 and b_2 determine the relative contribution of the length scales characterized by k_1 and k_2 , so that different scenarios, such as homogenous nucleation dominated by the ordering with the period k_1 or k_2 , can be studied [Figs. 1(b)–1(e)]. For example, by choosing a smaller value of b_1 or a bigger value of b_2 , the case of $\omega(k_1) > \omega(k_2) > 0$ can be obtained [Fig. 1(c)], and then the structure ordering of length scale k_1 is expected to be faster than that of length scale k_2 . If there is only one unstable length scale

[Figs. 1(d) and 1(e)], the structure ordering of the unstable length scale will appear and evolve first, which is followed by triggering the instability of the other length scale. Therefore the nucleated phase dominated by the fastest structure ordering will be a more kinetically accessible state. This is a kinetic origin of the formation of transient or metastable phase during the nucleation and growth process. Note that the studies in Refs. [14,24] only considered the case of $(b_1, b_2) = (0, 0)$. In our study, we will show when more parameters ε , $\bar{\psi}$, b_1 , and b_2 are changeable, the system has more pathways to lose its stability and evolves into nonlinear regime. Under some specific conditions, the ordering contribution by the two inherent length scales reaches a delicate equilibrium in the system, which may favor the formation of QCs.

III. RESULTS AND DISCUSSIONS

A. Phase diagram

Before investigating the kinetics of QC growth by numerically solving Eq. (2), we revisit the phase diagram of the system with its free energy in Eq. (1) by using PFC simulation in order to indicate clearly where the pathway of QC nucleation and growth is activated. The stable phase may appear in the phase diagram if its free energy is lower than the other phases considered in the PFC modeling with two length scales, given the parameters ε , $\bar{\psi}$, b_1 , and b_2 . The free energy calculations can be performed when the profiles of atomic density field $\psi(\vec{r}, t)$ representing the possible phases are substituted in Eq. (1), respectively. For example, the density field of all these phases (f -fold symmetry and even the Int phase) can also be created from the interference pattern [65],

$$|\psi_{\text{qc}}(\vec{r})|^2 = \frac{1}{f^2} \left| \sum_{n=0}^{f-1} e^{i\vec{k}_n \cdot \vec{r}} \right|^2, \quad \vec{k}_n = \left(\cos\left(\frac{2\pi n}{f}\right), \sin\left(\frac{2\pi n}{f}\right) \right), \quad (6)$$

where \vec{k}_n is the wave vector or the characteristic length scale. The efficiency of the free energy calculations can be improved by adopting a so-called projection method [66]. Since the stable phase is also corresponding to the minimum of the free energy functional in Eq. (1), described as $\delta F(\psi)/\delta \psi = 0$, we can initially generate a fluid phase with several seeds of Tri or QC phases and track their competitive growths by numerically solving Eq. (2) at each point $(\varepsilon, \bar{\psi})$ of the parameter space with $(b_1, b_2) = (0, 0)$. The final steady state may be viewed as an energetically favorable stable phase (see Supplemental Note 1 in [67]). Therefore, we can obtain a new equilibrium phase diagram, which includes four phases, i.e., liquid, QC, Tri, and Int phase with respect to two parameters $\varepsilon, \bar{\psi}$, as shown in Fig. 2(a). The coexistence regions are marked in gray. Each simulation has been run for more than 100,000 time steps to guarantee that the profile of the atomic density field is a steady state. We note that our phase diagram obtained here is a little different from the one reported in Ref. [24] wherein the Int phase does not appear. The enlarged detail in Fig. 2(a) shows the positions of several typical growth modes of QCs. Mode C located at $(\varepsilon, \bar{\psi}) = (0.25, -0.314)$ is known for defect-free one-step growth mode (see Movie S1 [67] for the recovered growth process) previously reported in Ref. [24]. Modes A and B are for two kinds of new

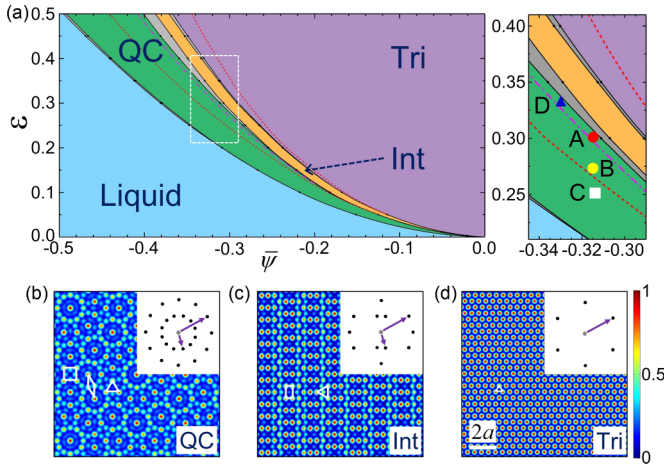


FIG. 2. Equilibrium phases explored by our PFC model, (a) Equilibrium phase diagram with stable liquid, Tri, dodecagonal QC, and Int phases is dependent on ε and $\bar{\psi}$ at $(b_1, b_2) = (0, 0)$. Coexistence regions are shaded in gray. The area between two red dotted lines is where the Int phase may appear during the Tri-QC competitive growth process, while the pink dash-dotted line indicates the linear instability threshold based on $\omega(k) = 0$. Enlarged detail in the white box is shown at the right site, wherein the positions of different modes, A-D, for the formation of QCs are marked, respectively. (b)–(d) The real-space patterns of three solid phases and their diffraction patterns (inset). The white polygons outline the unit cells of their respective tiling structures.

heterogeneous growth modes involving intermediate phases and a multistep behavior. Mode D located at $(\varepsilon, \bar{\psi}) = (0.33, -0.33)$ is for the homogeneous QCs nucleation mode.

To better focus on the multistep metastable behavior, we numerically find the range as indicated between the two red dotted lines in the phase diagram Fig. 2(a), where the Int phase appears as a metastable state or a stable phase by solving Eq. (2) with initially setting Tri and QC phases 50/50 distributed. It is clear that the region of Int phase that can

appear is larger than the region where it is a stable phase. Also, the spinodal-like instability threshold determined by the condition $-\varepsilon + 3\bar{\psi}^2 = 0$ discussed in Sec. II B is depicted as pink dash-dotted line in Fig. 2(a). The deeply quenched liquid becomes unstable with respect to any small modulations at the point D, which locates above the instability threshold and still in the region of QCs.

B. Heterogeneous QCs nucleation and growth

1. Single nucleus growth

As shown in Fig. 3, two different heterogeneous growth modes of QCs from one nucleus are studied [see Modes A,B in Fig. 2(a)]. In Mode A, the initialized QC nucleus firstly grows up steadily in the undercooled liquid [Fig. 3(a1) and 3(a2)]. Then when the nucleus tends to contact with other QC nuclei (due to the periodic boundary conditions), metastable Tri structures appear as a bridging phase at the QC-QC boundaries [Fig. 3(a3)], and transform into an Int structure later [Fig. 3(a4)]. A stable QC phase eventually occupies the whole system after $t = 1500$ [Fig. 3(a5)]. It clearly shows a multistep behavior of QC growth via the pathway of Tri \rightarrow Int \rightarrow QC.

In Mode B, we initially set one metastable Tri nucleus in the undercooled liquid to study the kinetics of forming QC phase. The QC structure is found to nucleate at the center of the growing Tri nucleus when the Tri nucleus grows up to a certain size [Fig. 3(b2)]. Then the Int structure nucleates at the QC-Tri boundary [Fig. 3(b3)], that is, the solid-liquid growth front of QC nucleus is surrounded by two layers of metastable states (Tri and Int layers). After the solid structures occupy the whole system, the Tri structure starts to vanish [Fig. 3(b4)], then the Int structure. Finally, we have a stable QC phase after $t = 1850$ [Fig. 3(b5)].

The growth processes observed in Fig. 3 are significantly different from the one-step growth mode reported in Ref. [24] [marked as Mode C in the phase diagram of Fig. 2(a)]. Modes A and B demonstrate that a multistep behavior clearly exists during nucleation and growth of QCs in the undercooled

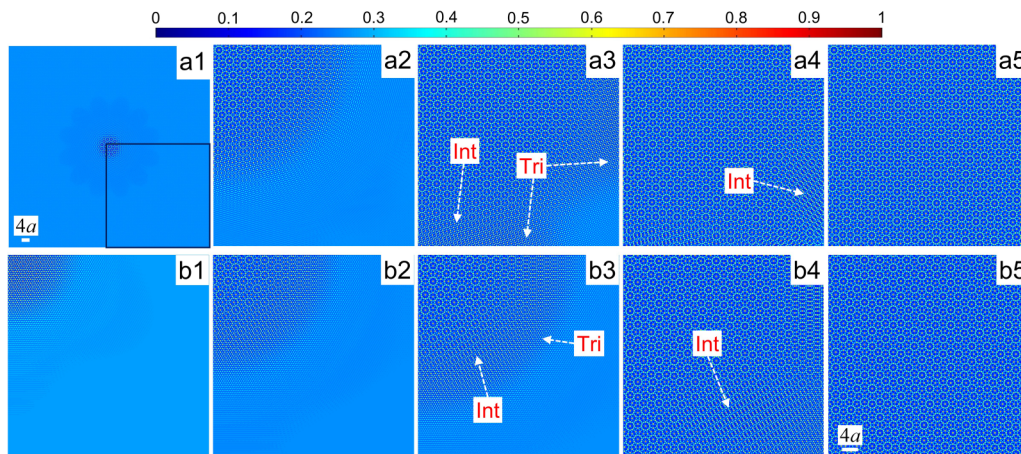


FIG. 3. Growth process of QCs in the undercooled liquid matrix with one nucleus. (a1)–(a5) are the atomic density profiles for the growth of a QC nucleus at $(\varepsilon, \bar{\psi}) = (0.30, -0.315)$, corresponding to Mode A in Fig. 2(a) at $t = 50, 400, 600, 900, 1500$, respectively. (b1)–(b5) are for the growth of a Tri nucleus at $(\varepsilon, \bar{\psi}) = (0.2705, -0.315)$, corresponding to Mode B in Fig. 2(a) at $t = 500, 750, 900, 1500, 1850$, respectively. See Movie S2 [67] for the evolution detail of the whole system. Note that (a2)–(a5) and (b1)–(b5) only show a quarter of the simulated system in (a1).

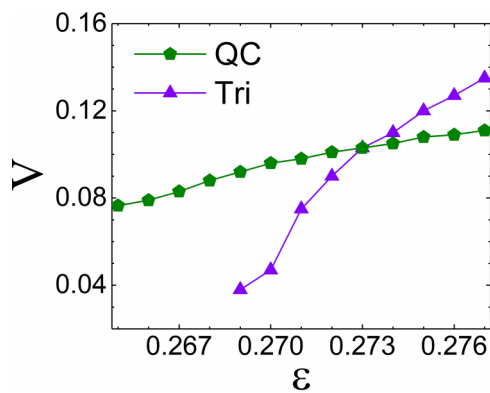


FIG. 4. The calculated average growth rate V normalized by $a/\Delta t$ of Tri and QC nuclei versus the degree of undercooling ε during one-step and multistep growth modes from the initially undercooled liquid at $\bar{\psi} = -0.315$. The red circle marks the point where Tri structure is unstable in the liquid and will transform to QC in the first 500 time steps.

liquid. Tri structure is formed in the liquid-QC interface first, which is followed by a “Tri-Int-QC” two-step structural phase transformation, and this multistep process contributes to the growth of the QC structure in the liquid (see Movie S1 and S2 [67] for more growth information of the one-step mode and the multistep mode). To understand the thermodynamic and kinetic origins of the heterogeneous QC growth involving metastable phases and a multistep behavior, we roughly estimate the free energy change in a local region where liquid, Tri, Int and QC phases appear sequentially during the growth of QC in Fig. 3. We found that $E_{QC} < E_{Int} < E_{Tri} < E_{Liquid}$. Usually the pure Tri or Int phase in Fig. 3 is not energetically favorable. However, when QC nuclei with different orientations coexist, if the energy gap between QC and Tri phases is small and the QC-Tri interfacial energy is lower than that between QC nuclei with different orientations, the metastable Tri phase nucleating at the QC-QC boundaries may emerge as a bridging layer between QC nuclei with different orientations to reduce the total free energy of the system. Similarly, the Int structure nucleating at the QC-Tri boundaries may also be energetically favorable when the QC-Int interfacial energy is lower than the QC-Tri interfacial energy. Overall, the multistep metastable phenomena in QC growths are more likely to be found near the Tri-QC phase boundary in the phase diagram than that far away from the boundary according to our simulations. The thermodynamic origin shares a similar mechanism reported in other nonclassical nucleating systems [45]. When the relative magnitude of the free energy of these solid phases is small, the bulk free energy increase due to the appearance of the metastable phase can be counterbalanced by the decrease of some solid-solid interfacial energy.

To examine the kinetic origin of the multistep growth mode, we perform simulations of single Tri or QC nucleus of equal size growing in the undercooled liquid with the same $\bar{\psi} = -0.315$ under different values of ε , and measure their average growth rates during the initial 500 dimensionless time steps. As shown in Fig. 4, the simulated result indicates that the average growth rate of both Tri and QC nuclei increases with the increase of ε but their trends are different. In addition,

when ε decreases to a critical value, the growth rate of QC nucleus is much larger than that of the Tri nucleus and therefore the newly generated QC nucleus catches up with the Tri-liquid boundary and exhibits a one-step mode afterwards. We should note that the kinetics shown in Fig. 4 is mainly determined by thermodynamics since PFC kinetic equation is overdamped. The growth velocity of a new phase is roughly proportional to the mobility of phase interface and the total thermodynamic driving force, which includes the bulk free energy differences and the interfacial energy between the new and old phases. We roughly compared the bulk free energy difference between metastable phases and the final stable quasicrystal phase at different values of ε , and found that these bulk free energy differences increase as increasing the value of ε . The driving force and the growth velocity is larger at higher ε , consistent with the result in Fig. 4. However the fact that the growth velocity of the Tri nuclei becomes larger above a critical value of ε than that of the QC nuclei should be consistent with a larger total thermodynamic driven force for the Tri nuclei than that for the QC nuclei. It is possible when the interfacial energy between the Tri and liquid phases is smaller than that of the interfacial energy between the QC and liquid phases. It demonstrates that a faster growth rate of the nucleus makes it kinetically more accessible. If the growth rate of an initially seeded nucleus is larger than that of the nucleus subsequently formed within it, a multistep growth mode can happen. Our numerical results confirm that given larger degree of undercooling ($\varepsilon = 0.2715$), the metastable layers become thicker because the growth rate of Tri is much faster. In addition, taking the growth of a metastable Tri nucleus in the undercooled liquid as an example, even though the growth rate of the QC structure is faster in Mode B, the multistep phenomenon is still observable, because the existent Tri structure has to spend extra time to transform into QC first, as shown in Fig. S3 [67]. That is, for the one-step mode of the QC formation, the degree of undercooling has to be low enough to make sure that the growth rate of the QC nucleus is fast enough to avoid the emergence of metastable Tri state in the growth front. Otherwise, the multistep mode will appear. In a word, the growth modes of QC from undercooled liquid depend on the difference of the growth rates between the stable QC and the metastable Tri nuclei.

The result in Fig. 4 indicates that multistep growth of QC in Mode B appears when the metastable Tri nuclei is kinetically more accessible and its growth rate is larger. A similar two-step growth mode is reported in MD simulations [25], which suggests that the icosahedral clusters formed in the growth front first give rise to the growth of dodecagonal QCs. The MD result in Ref. [40] shows that the metastable body-centered cubic (bcc) phase nucleates first in the undercooled liquid, followed by the transformation to face-centered cubic (fcc) ordering when the bcc nucleus reaches a critical size, and metastable bcc-like ordering can also be found around the interface of the critical fcc nucleus. We should note that the kinetic effect on multistep growth of QC reported in Fig. 4 is mainly of thermodynamic origin while the multistep growth behavior in the MD results of Refs. [25,40] contains not only kinetic effect driven by thermodynamics but also purely kinetic effect and nucleation process.

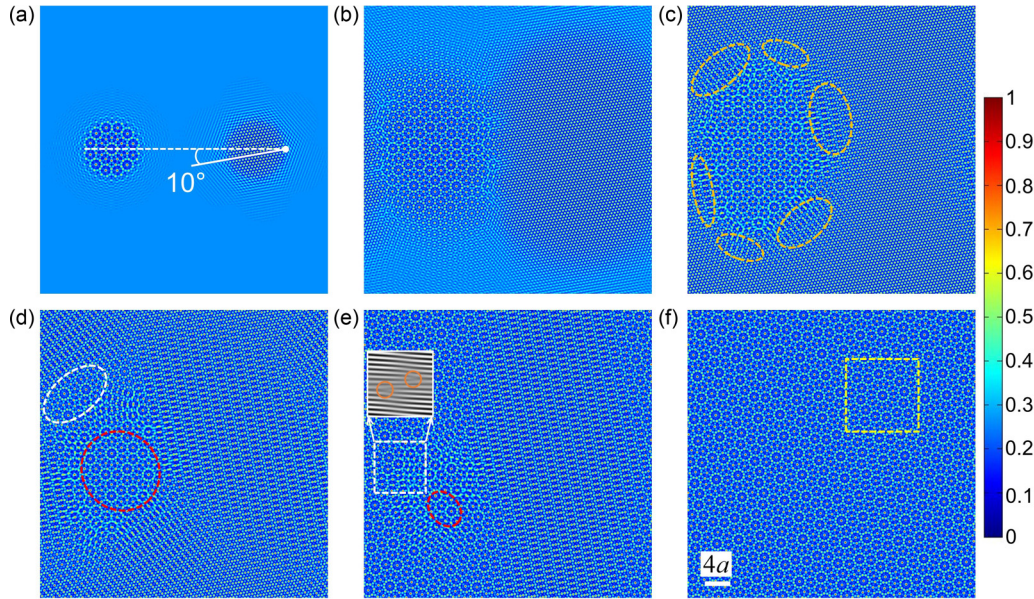


FIG. 5. The competitive growth between a QC nucleus and a Tri nucleus in a fluid phase shows a typical “liquid-Tri-Int-QC” transformation pathway at $(\varepsilon, \psi) = (0.305, -0.315)$. (a) Initial configuration of the simulated system with a QC nucleus and a Tri nucleus of the same size but different orientations. (b)–(f) are snapshots at different dimensionless time steps $t = 160, 1000, 1800, 3000, 6400$, respectively. The ellipses in (c) mark the nucleated sites of Int structures, while the red and white ellipses in (d),(e) mark the shrinking QC domain with the initial orientation and the generated new-QC domain with a different orientation, respectively. In (e), the inset indicates the dislocations in the marked white square box. Configuration evolutions in the yellow box of (f) will be employed to study the details of two-step structural transformations in Fig. 9. Note that the simulating domain is $512\Delta x \times 512\Delta x$. See Movie S3 [67] for more evolution details.

2. Competitive growth of QC and Tri nuclei

To further study the emergence of the metastable Int phase and more kinetic details during the multistep growth of QCs, the competitive growth between one QC and one metastable Tri nucleus has been studied, as shown in Fig. 5. By setting the orientation difference of these two nuclei [Fig. 5(a)], the transformation information, including whom the new phase generates from, can be detected directly. First, the QC nucleus and Tri nucleus both grow up and collide [Fig. 5(b)], where the Tri nucleus grows obviously faster in accord with the growth rate analysis in Fig. 3. After these two nuclei occupy the whole system, the Int nuclei with three different orientations (marked by ellipses) emerge along the QC-Tri boundaries [Fig. 5(c)]. Then the remaining Tri domain is rapidly eaten up by Int domains with two dominating orientations. Meanwhile, a new QC nucleus with its orientation different from the original QC nucleus appears at the QC-Int boundary, and then takes over the original QC gradually [Fig. 5(d)] via the motion of the so-called dislocations in QCs, which can be detected by a particular method [68,69], as shown in the inset of Fig. 5(e). The newly generated Int structure survives for a longer time, and finally a stable QC is formed [Fig. 5(f)].

It is known that the orientation relation between the product phase and the mother phase in the structural transformation is crucial, because it significantly influences the coherency of the two-phase boundary, defect structures at the incoherent interface and their interfacial energy. As shown in Fig. 5(c), it is recognized that the orientation of the newly generated Int nuclei is inherited from the original Tri nucleus, not from the original QC structure. Similarly, the orientation of the newly generated QC nucleus in Fig. 5(d) is determined

by the orientation of its adjacent Int structure, which is different from that of the original QC nucleus. Overall, a typical “liquid-Tri-Int-QC” three-step QC growth is presented here. The results in Fig. 5 clearly demonstrate that a multistep mode involving metastable Tri and Int phases can be frequently observed during the formation of QC from a liquid phase. This nonclassical transformation pathway can trigger secondary nucleation of QC and drastically influence the orientation between QC nuclei, different from the classical nucleation pathway, wherein a single step transition from mother phase to product phase is assumed.

C. Homogeneous QC nucleation and growth

Another pathway for formation of QC from a liquid phase is homogeneous nucleation and growth. It would be interesting to explore whether the metastable and multistage growth kinetics of QCs occur during homogeneous nucleation and growth or not. In the case of homogeneous nucleation, the initially uniform liquid phase is unstable and decays spinodally. Figure 6 plots the growth rate versus the wave number for the spinodal-like instability by conducting the linear stability analysis. According to the analysis in Sec. II B, the magnitude of growth rate of the two length scale ordering can be adjusted by changing the values of b_1, b_2 , and ε, ψ . The plot in Fig. 6(a) shows that there are two kinds of length scale ordering and the growth rate of the short length scale ordering (k_2) is much larger than that of the longer one (k_1). Figure 6(b) shows that the dispersion relation can be altered by the parameters b_1, b_2 . The growth rate for the long length scale ordering could be larger than that of the short one. The ordering state with faster growth rate is kinetically more accessible.

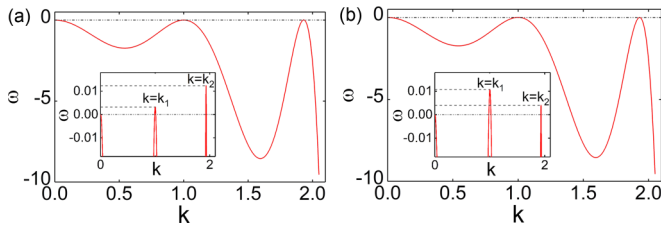


FIG. 6. Dispersion relation $\omega(k)$ at the state point $(\varepsilon, \bar{\psi}) = (0.33, -0.33)$ for (a) $(b_1, b_2) = (0, 0)$ and for (b) $(b_1, b_2) = (-0.001, 0.0003)$. In these two cases, both length scales (k_1 and k_2) are unstable, but the growth rate of the smaller length scale in (a) is much larger than that for the longer one, while in (b) the case is the opposite. The insets show the details near $\omega = 0$. The corresponding simulated results are shown in Figs. 7 and 8.

Figure 7 shows the evolution of QC growth during the homogeneous nucleation process for Mode D in Fig. 2(a) with the dispersion relation in Fig. 6(a). Consistent with the analysis in Fig. 6(a), the small length scale crystal (i.e., Tri phase) forms first due to the faster growth rate of such length scale ordering, and the subsequent competing and coupling of two length scale orderings lead to formation of some QC precursors [i.e., local quasicrystalline structures, marked by red circles in Fig. 7(b)] in the undercooled liquid. Later, as the system further evolves, both length scale orderings play a comparable role. The QC structure then nucleates near the grain boundary of Tri phase [Fig. 7(c)], where the high interfacial energy can easily trigger the nucleation of QCs. After the appearance of the QC phase, the existent Tri structure transforms to the stable QC phase via the “Tri-Int-QC” two-step transitions [Figs. 7(d) and 7(e)], and finally the stable QC is formed [Fig. 7(f)].

According to the result in Fig. 6(b), the growth rate of the long length scale ordering could be larger than that of the

short one by altering the parameters b_1, b_2 . Figure 8 shows the evolution of QC growth from an initially uniform liquid phase with the dispersion relation in Fig. 6(b). The Tri crystal with a larger lattice constant reciprocal to k_1 is expected to form first, but it is in fact not observable before the nucleation of QC structures [Figs. 8(b) and 8(c)] due to the further evolution of two length scale orderings. Then metastable Tri structures occur at the QC-liquid boundary to reduce the boundary energy [Fig. 8(d)], and finally transform to stable QC through metastable Int states [(Figs. 8(e) and 8(f)].

The results presented in Figs. 7 and 8 suggest that there are also multistep modes involving metastable Tri and Int phases during homogeneous QC growth. The relative contribution of two length scale orderings affects the growth dynamics of QCs, especially in the earliest stage of nucleation. We also find that QCs can always be recovered when two length scales comparably contribute to the system, no matter which length scale dominates in the beginning.

The metastable phenomena may have qualitative similarity to the two-step theory proposed in Refs. [26,27], where QCs are quite far from the onset of instability and form from a periodic state via the nonlinear time-dependent process. However, our results further show the fascinating multistep metastable behavior to form QCs and an involved metastable Int state arising during the transition from a periodic structure to a quasicrystalline structure. In the following sections, the structure of Int and its correlation with Tri and QC structures will be studied.

D. Structural correlation of “Tri-Int-QC” transitions

The “liquid→Tri→Int→QC” multistep growth pathway of QCs is ubiquitous in all our simulated cases. As shown in Figs. 2(b)–2(d), the diffraction patterns of three solid phases

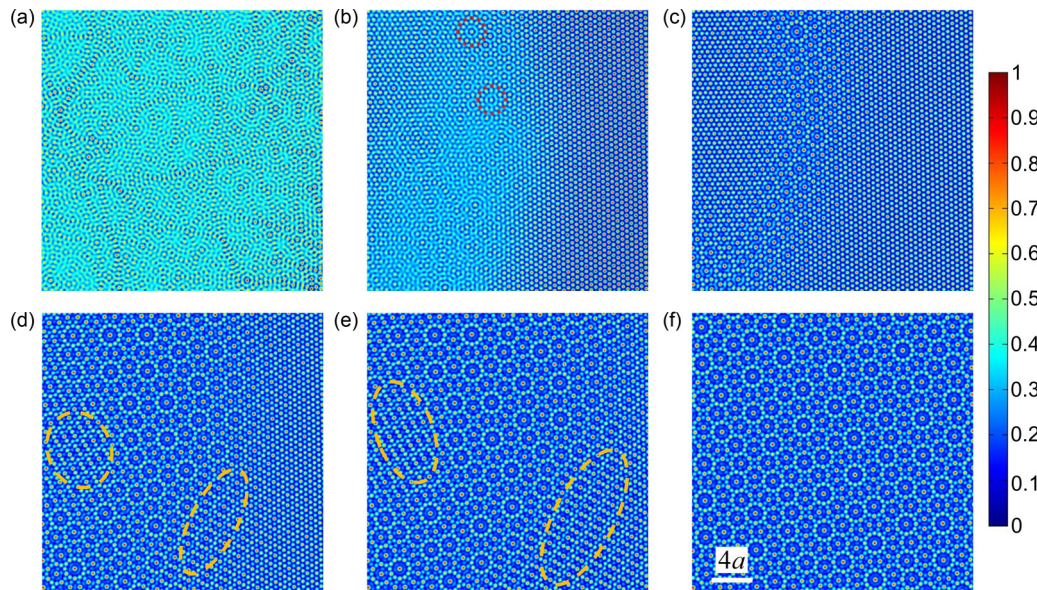


FIG. 7. Local snapshots of the homogeneous nucleation process for Mode D in Fig. 2(a) with the dispersion relation displayed in Fig. 6(a). (a)–(f) are snapshots at $t = 3000, 3068, 3160, 3420, 3580, 5560$, respectively. The red circles in (b) mark the nucleation precursors of QCs with local quasicrystalline structures, and the orange ellipses in (d) and (e) mark the emergent Int structures. See Movie S4 [67] for the evolution detail of the whole system.

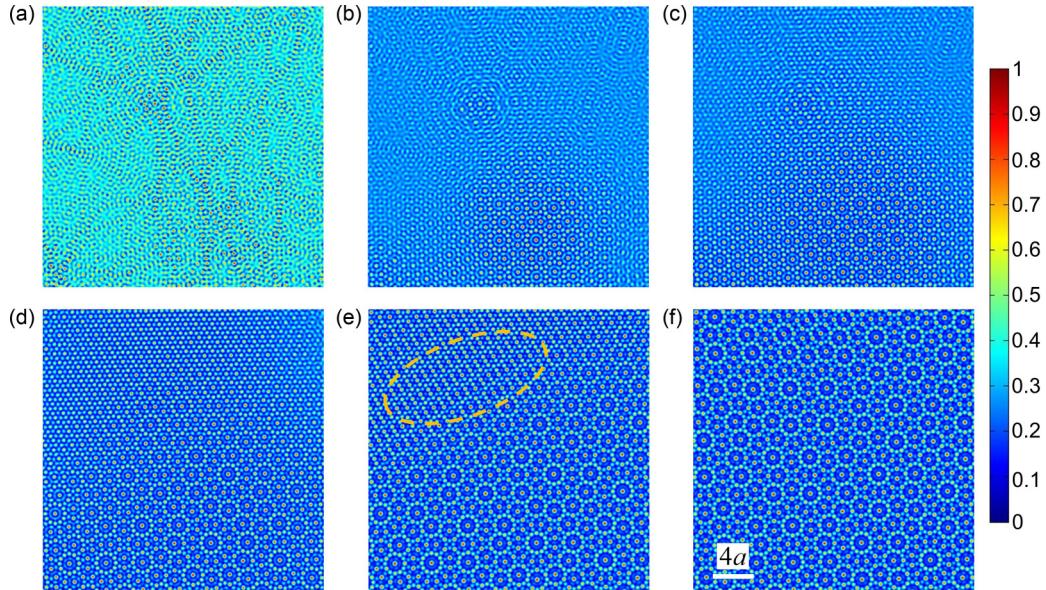


FIG. 8. Local snapshots of the homogeneous nucleation process for the case with $(\varepsilon, \bar{\psi}) = (0.33, -0.33)$ and $(b_1, b_2) = (-0.001, 0.0003)$. The dispersion relation in this case is displayed in Fig. 6(b). (a)–(f) are snapshots at $t = 9310, 9340, 9350, 9360, 9390, 9620$, respectively. The orange ellipse in (e) marks the emergent Int structure. See Movie S5 [67] for the evolution detail of the whole system.

apparently have structural analogy, wherein the diffraction peaks of the Int phase include those of the Tri phase, while it is part of those of QC phase. In addition, during the “Tri-Int-QC” structural transformation, the product phase and parent phase always have the same orientation. This evidence indicates that there is intrinsic structural correlation between these three solid phases related to their deeper hidden transition mechanism, although we can qualitatively understand that the multistep behavior is energetically favorable or kinetically more accessible.

In this section, we select a region of the simulating system in Fig. 5 to analyze the structural evolution by employing the circularly averaged structure factor $S(k)$ [70], defined as $S(k) = \langle |\hat{\psi}_k|^2 \rangle$, where $\hat{\psi}_k$ is the Fourier transform of density field $\psi(\vec{r})$. Figure 9 shows how the structure factor changes with time during the dynamic process of “Tri-Int-QC” structural transformation. The result in Fig. 9 clearly exhibits the two-step behavior of two length scale orderings. Note that the locations of two peak values of $S(k)$, k_1 , and k_2 , are two intrinsic length scales that are necessary to form QCs [14,24]. At the initial stage, the amplitude of $S(k_2)$ quickly reaches a peak while the amplitude of $S(k_1)$ is almost zero before $t = 800$, which corresponds to the formation of Tri phase with the period k_2 . After $t = 800$, the amplitude of $S(k_1)$ grows up gradually with the decrease of $S(k_2)$ until both $S(k_1)$ and $S(k_2)$ reach a plateau and $S(k_2) > S(k_1)$ in the range from $t = 2000$ to $t = 5600$, which is corresponding to the formation of the Int phase. After $t = 5600$, $S(k_1)$ keeps increasing with continuous decrease of $S(k_2)$. At $t = 6400$, they both become stable, which corresponds to the formation of a final stable QC structure. It is interesting to note that the profile of the structure factor for Int and QC structures [see rows $t = 2000$ and $t = 6400$ of Fig. 9(b)] is analogous, where the difference is that $S(k_2) > S(k_1)$ for the Int structure while $S(k_1) > S(k_2)$ for the QC structure.

The evolving details of the structural factor demonstrate that the competing and coupling between the two intrinsic length scale orderings give rise to the structural origin of the multistep growth of QC, wherein the relative increasing (decreasing) contribution of long (short) length scale k_1 (k_2) leads to formation of Tri structure first, then followed by the Int structure, and finally the formation of the stable QC phase.

E. Tiling structure of Int phase

One-dimensional (1D) quasicrystalline order is argued to exit between a 2D QC and a 2D crystal [71], because an intermediate phase between crystals and QCs, which is shown containing periodic ordering and quasicrystalline ordering,

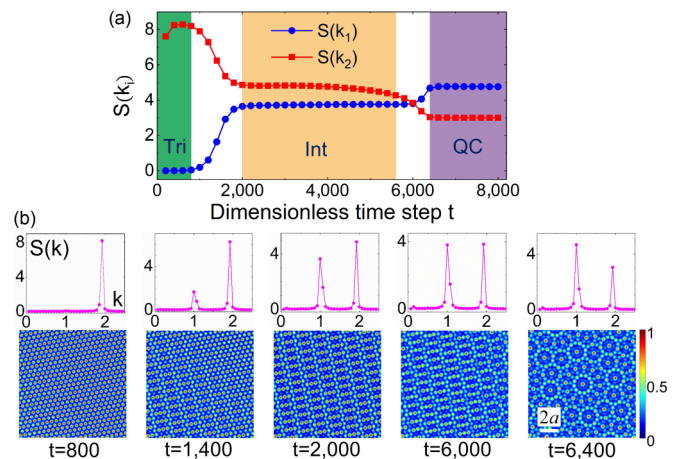


FIG. 9. Dynamic process of “Tri-Int-QC” structural transformation in a specific region marked as yellow box in Fig. 5(f). (a) Evolution of peak values of averaged structure factor $S(k_1)$ and $S(k_2)$ during the transition process. (b) Upper row: circularly averaged structure factor. Bottom row: real-space snapshots.

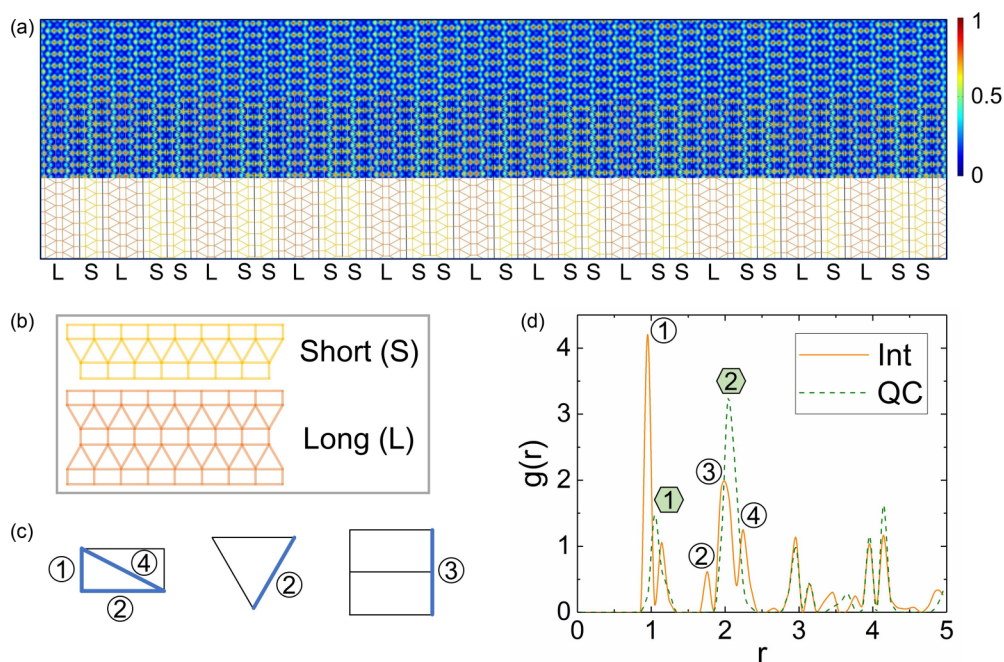


FIG. 10. Structural characterization of the Int phase. (a) The tiling structure of the calculated Int phase at $(\varepsilon, \bar{\psi}) = (0.32, -0.315)$. (b) Two unit cells of the aperiodic sequence. (c) Schematic plots of the characteristic length scales of Int structure. (d) Radial distribution functions of Int structure in (a), and QC structure at $(\varepsilon, \bar{\psi}) = (0.26, -0.315)$. Note that r is normalized by the unit short length scale $a/(2 \cos(\pi/12))$.

has been reported in the quasicrystalline substrate system [28]. In our multistep simulation results, the Int structure always happens as an intermediate state during “Tri-QC” structural transformations. Thus it is also expected to be a structure bridge of both periodicity and quasiperiodicity, which will be illustrated by structural characterization in this section.

In Fig. 10, we obtain the formation of a large Int structure at $(\varepsilon, \bar{\psi}) = (0.32, -0.315)$ in a system of $2048\Delta x \times 2048\Delta x$ and characterize this structure by tiling analysis and radial distribution function $g(r)$. Figure 10(a) shows that in one direction, rectangular chains insert irregularly and make the random sequence of rectangular-triangular array which contains two unit cells, short (S) and long (L) as shown in Fig. 10(b). We also surprisingly find that the sequence exhibits aperiodic order. Moreover, in all the “Tri-Int-QC” structural transformations of our multistep growth cases, we find the generated Int and QC structures own the same orientation as the parent Tri structure. Specifically, the orientation parallel to transition direction at “Tri-Int” or “Int-QC” boundaries aligns with a specific orientation of Int structure, i.e., the aperiodic orientation. It is energetically favorable that two orientations of 2D Int structure could match with one periodic orientation of Tri structure and one aperiodic orientation of QC structure at the same time. These evidences indicate that the aperiodicity of Int structure is suggested to be the unique quasiperiodic order of dodecagonal QC. Two unit cells and their shortest length scales in the Int structure shown as the sketches in Figs. 10(b) and 10(c) are identified from the calculated profile of the radial distribution function $g(r)$ [Fig. 10(d)]. In comparison with the $g(r)$ of QC structure, which has two dominant shortest length scale peaks, the $g(r)$ of Int structure has three separate peaks at the second shortest length scale, which is caused by the existence of rectangular

units. The prevalent rectangular unit, which is constructed by both short and long characteristic length scales, exhibits a perfect linking unit between Tri structure (formed by short length scale) and QC structure (dominated by long length scale). This indicates that the rectangular unit plays a crucial role in formation of the Int structure and eventually causing the two-step structural transformations.

Furthermore, by changing the intrinsic length scales of the model to $k_1 = 2\pi/a$ and $k_2 = 4\pi \cos(\pi/5)/a$, decagonal (tenfold) QC can be obtained. In this condition, multistep growth behavior of QCs also exists in certain parameter space and a new Int structure of decagonal QC is also found, as shown in Fig. S4 [67]. Similarly, two unit cells, containing isosceles triangle and rectangle units, can be recognized to define this structure. We note that the Int phase in our simulations is different from the intermediate phase found previously in the quasicrystalline substrate system [28], although they both bridge the periodicity and quasiperiodicity. The Archimedean tiling $(3^3 \cdot 4^2)$ structure in Ref. [28] is the result of mechanical cooperation of the particle-particle and particle-substrate interactions, while our Int phase exists inherently in the two length scale models and can be stable in certain parameter space. On the other hand, from the perspective of tiling and unit cell analysis, our Int phase can be constructed by two shortest characteristic length scales, while the Archimedean tiling structure [28], even though having simple square and triangle units, is hard to construct as it is such a long-range aperiodic sequence in one direction with some simple two-length-scale potential. Moreover, a similar structure, called the compressed hexagonal phase, has been reported in a cluster QC system by molecular dynamics simulations [16], while we suggest that it is a 1D aperiodic structure based on this work.

IV. CONCLUSIONS

In summary, an unconventional multistep growth behavior of QCs due to the existence of the metastable Tri and Int phases is discovered in both heterogeneous and homogeneous nucleation and growth processes investigated by phase field crystal simulations. In comparison to the one-step growth mode of QCs [24], these new growth modes of QCs are found in a specific parameter space near the Tri-QC boundary in the phase diagram. In this parameter space, the metastable Tri phase is kinetically more accessible if the growth rate of one length-scale ordering is much larger than the other based on the linear stability analysis of the undercooled fluid phase. Furthermore, in the presence of QC-Tri phase coexistence the appearance of the metastable Int phase at the QC-Tri boundary can be energetically favorable. Because the newly formed QC-Int interface may further reduce the QC-Tri interfacial energy and the distortion energy of the lattice mismatch at the QC-Tri boundary when the relative magnitude of the free energy difference of three solid phases is relatively small, the increase of the bulk free energy of the Int phase is offset by reducing

the excess energy due to the QC-Tri phase coexistence. The metastable Int phase that always appears at the “Tri-QC” transition pathway has the intrinsic structural correlation with Tri and QC phases. Specifically, the Int structure is proven to be a 1D aperiodic structure to bridge the Tri and QC structure by the analysis of structure factor evolution, radial distribution functions, and tiling construction. Our results presented here demonstrate that the metastable multistep growth behavior is a key feature of a nonequilibrium phase transition during the nucleation and growth of QCs.

ACKNOWLEDGMENTS

This work was supported by the Strategic Priority Research Program of the Chinese Academy of Sciences (Grant No. XDB22040502), the National Natural Science Foundation of China (Grant No. 11672285), the Collaborative Innovation Center of Suzhou Nano Science and Technology, and the Fundamental Research Funds for the Central Universities (WK2090050043).

-
- [1] D. Shechtman, I. Blech, D. Gratias, and J. W. Cahn, *Phys. Rev. Lett.* **53**, 1951 (1984).
- [2] D. Levine and P. J. Steinhardt, *Phys. Rev. Lett.* **53**, 2477 (1984).
- [3] W. Steurer, *Acta Crystallogr. Sect. A* **74**, 1 (2018).
- [4] X. Zeng, G. Ungar, Y. Liu, V. Percec, A. E. Dulcey, and J. K. Hobbs, *Nature (London)* **428**, 157 (2004).
- [5] K. Hayashida, T. Dotera, A. Takano, and Y. Matsushita, *Phys. Rev. Lett.* **98**, 195502 (2007).
- [6] D. V. Talapin, E. V. Shevchenko, M. I. Bodnarchuk, X. Ye, J. Chen, and C. B. Murray, *Nature (London)* **461**, 964 (2009).
- [7] S. Fischer, A. Exner, K. Zielske, J. Perlich, S. Deloudi, W. Steurer, P. Lindner, and S. Forster, *Proc. Natl. Acad. Sci.* **108**, 1810 (2011).
- [8] C. Xiao, N. Fujita, K. Miyasaka, Y. Sakamoto, and O. Terasaki, *Nature (London)* **487**, 349 (2012).
- [9] J. Zhang and F. S. Bates, *J. Am. Chem. Soc.* **134**, 7636 (2012).
- [10] Y. Nagaoka, H. Zhu, D. Eggert, and O. Chen, *Science* **362**, 1396 (2012).
- [11] W. Steurer, *Acta Crystallogr. Sect. A* **61**, 28 (2005).
- [12] C. L. Henley, *Random Tiling Models in Quasicrystals: The State of the Art*, edited by D. P. DiVincenzo and P. J. Steinhardt (World Scientific, Singapore, 1991), p. 429.
- [13] A. R. Denton and H. Löwen, *Phys. Rev. Lett.* **81**, 469 (1998).
- [14] R. Lifshitz and D. M. Petrich, *Phys. Rev. Lett.* **79**, 1261 (1997).
- [15] K. Barkan, H. Diamant, and R. Lifshitz, *Phys. Rev. B* **83**, 172201 (2011).
- [16] K. Barkan, M. Engel, and R. Lifshitz, *Phys. Rev. Lett.* **113**, 098304 (2014).
- [17] P. Subramanian, A. J. Archer, E. Knobloch, and A. M. Rucklidge, *Phys. Rev. Lett.* **117**, 075501 (2016).
- [18] M. Engel and H. R. Trebin, *Phys. Rev. Lett.* **98**, 225505 (2007).
- [19] M. Engel, P. F. Damasceno, C. L. Phillips, and S. C. Glotzer, *Nat. Mater.* **14**, 109 (2015).
- [20] T. Dotera, T. Oshiro, and P. Zihlerl, *Nature (London)* **506**, 208 (2014).
- [21] K. Nagao, T. Inuzuka, K. Nishimoto, and K. Edagawa, *Phys. Rev. Lett.* **115**, 075501 (2015).
- [22] L.-H. Tang and M. V. Jarić, *Phys. Rev. B* **41**, 4524 (1990).
- [23] A. Kiselev, M. Engel, and H. R. Trebin, *Phys. Rev. Lett.* **109**, 225502 (2012).
- [24] C. V. Achim, M. Schmiedeberg, and H. Lowen, *Phys. Rev. Lett.* **112**, 255501 (2014).
- [25] A. S. Keys and S. C. Glotzer, *Phys. Rev. Lett.* **99**, 235503 (2007).
- [26] A. J. Archer, A. M. Rucklidge, and E. Knobloch, *Phys. Rev. Lett.* **111**, 165501 (2013).
- [27] A. J. Archer, A. M. Rucklidge, and E. Knobloch, *Phys. Rev. E* **92**, 012324 (2015).
- [28] J. Mikhael, J. Roth, L. Helden, and C. Bechinger, *Nature (London)* **454**, 501 (2008).
- [29] J. Mikhael, G. Gera, T. Bohlein, and C. Bechinger, *Soft Matter* **7**, 1352 (2011).
- [30] S. Karthika, T. K. Radhakrishnan, and P. Kalaichelvi, *Crystr. Growth Des.* **16**, 6663 (2016).
- [31] J. Lee, J. Yang, S. G. Kwon, and T. Hyeon, *Nat. Rev. Mater.* **1**, 16034 (2016).
- [32] L. Gránásy, G. I. Tóth, J. A. Warren, F. Podmaniczky, G. Tegze, L. Rátkai, and T. Pusztai, *Prog. Mater. Sci.* **106**, 100569 (2019).
- [33] L.-Q. Chen and A. G. Khachatryan, *Phys. Rev. B* **44**, 4681 (1991).
- [34] Y. Ni, Y. M. Jin, and A. G. Khachatryan, *Acta Mater.* **55**, 4903 (2007).
- [35] Y. Ni and A. G. Khachatryan, *Nat. Mater.* **8**, 410 (2009).
- [36] T. W. Heo, D. S. Shih, and L.-Q. Chen, *Metall. Mater. Trans. A* **45**, 3438 (2014).
- [37] S. Nag, Y. Zheng, R. E. A. Williams, A. Devaraj, A. Boyne, Y. Wang, P. C. Collins, G. B. Viswanathan, J. S. Tiley, B. C. Muddle, R. Banerjee, and H. L. Fraser, *Acta Mater.* **60**, 6247 (2012).

- [38] Y. Zheng, R. E. A. Williams, D. Wang, R. Shi, S. Nag, P. Kami, J. M. Sosa, R. Banerjee, Y. Wang, and H. L. Fraser, *Acta Mater.* **103**, 850 (2016).
- [39] A. Boyne, D. Wang, R. P. Shi, Y. Zheng, A. Behera, S. Nag, J. S. Tiley, H. L. Fraser, R. Banerjee, and Y. Wang, *Acta Mater.* **64**, 188 (2014).
- [40] P. R. ten Wolde, M. J. Ruiz-Montero, and D. Frenkel, *Phys. Rev. Lett.* **75**, 2714 (1995).
- [41] P. Tan, N. Xu, and L. Xu, *Nat. Phys.* **10**, 73 (2013).
- [42] C. Guo, J. Wang, J. Li, Z. Wang, and S. Tang, *J. Phys. Chem. Lett.* **7**, 5008 (2016).
- [43] S. Tang, J. C. Wang, B. Svendsen, and D. Raabe, *Acta Mater.* **139**, 196 (2017).
- [44] N. D. Loh, S. Sen, M. Bosman, S. F. Tan, J. Zhong, C. A. Nijhuis, P. Kral, P. Matsudaira, and U. Mirsaidov, *Nat. Chem.* **9**, 77 (2017).
- [45] Y. Peng, F. Wang, Z. Wang, A. M. Alsayed, Z. Zhang, A. G. Yodh, and Y. Han, *Nat. Mater.* **14**, 101 (2015).
- [46] M. Zu, P. Tan, and N. Xu, *Nat. Commun.* **8**, 2089 (2017).
- [47] K. R. Elder, M. Katakowski, M. Haataja, and M. Grant, *Phys. Rev. Lett.* **88**, 245701 (2002).
- [48] K. R. Elder and M. Grant, *Phys. Rev. E* **70**, 051605 (2004).
- [49] Y. M. Jin and A. G. Khachatryan, *J. Appl. Phys.* **100**, 013519 (2006).
- [50] J. Swift and P. C. Hohenberg, *Phys. Rev. A* **15**, 319 (1977).
- [51] M. C. Cross and H. Greenside, *Pattern Formation and Dynamics in Nonequilibrium Systems* (Cambridge University Press, Cambridge, 2009).
- [52] K. R. Elder, N. Provatas, J. Berry, P. Stefanovic, and M. Grant, *Phys. Rev. B* **75**, 064107 (2007).
- [53] S. van Teeffelen, R. Backofen, A. Voigt, and H. Lowen, *Phys. Rev. E* **79**, 051404 (2009).
- [54] K. A. Wu, A. Adland, and A. Karma, *Phys. Rev. E* **81**, 061601 (2010).
- [55] M. Greenwood, N. Provatas, and J. Rottler, *Phys. Rev. Lett.* **105**, 045702 (2010).
- [56] S. K. Mkhonta, K. R. Elder, and Z. F. Huang, *Phys. Rev. Lett.* **111**, 035501 (2013).
- [57] P. Stefanovic, M. Haataja, and N. Provatas, *Phys. Rev. Lett.* **96**, 225504 (2006).
- [58] V. Heinonen, C. A. Achim, K. R. Elder, S. Buyukdagli, and T. Ala-Nissila, *Phys. Rev. E* **89**, 032411 (2014).
- [59] A. Skaugen, L. Angheluta, and J. Viñals, *Phys. Rev. Lett.* **121**, 255501 (2018).
- [60] M. Salvalaglio, A. Voigt, and K. R. Elder, *npj Comput. Mater.* **5**, 48 (2019).
- [61] J. Rottler, M. Greenwood, and B. Ziebarth, *J. Phys. Condens. Matter* **24**, 135002 (2012).
- [62] S. Savitz, M. Babadi, and R. Lifshitz, *IUCrJ* **5**, 247 (2018).
- [63] L. Q. Chen and J. Shen, *Comput. Phys. Commun.* **108**, 147 (1998).
- [64] M. Lavrskyi, H. Zapolsky, and A. G. Khachatryan, *npj Comput. Mater.* **2**, 15013 (2016).
- [65] B. Freedman, R. Lifshitz, J. W. Fleischer, and M. Segev, *Nat. Mater.* **6**, 776 (2007).
- [66] K. Jiang, J. Tong, P. Zhang, and A. C. Shi, *Phys. Rev. E* **92**, 042159 (2015).
- [67] See Supplemental Material at <http://link.aps.org/supplemental/10.1103/PhysRevMaterials.4.023403> for stability of Tri and Int phase, Growth of QCs with and without multi-layer growth front, and movies describing detailed growth behavior of QCs.
- [68] L. Korkidi, K. Barkan, and R. Lifshitz, in *Aperiodic Crystals*, edited by S. Schmid, R. L. Withers, and R. Lifshitz (Springer, New York, 2013), p. 117.
- [69] M. Schmiedeberg, C. V. Achim, J. Hielscher, S. C. Kapfer, and H. Lowen, *Phys. Rev. E* **96**, 012602 (2017).
- [70] N. Provatas and K. R. Elder, *Phase Field Methods in Materials Science and Engineering* (Wiley-VCH, Weinheim, 2010).
- [71] S. C. Glotzer and A. S. Keys, *Nature (London)* **454**, 420 (2008).